Energies **2010**, *3*, 847-865; doi:10.3390/en3040847

OPEN ACCESS

energies

ISSN 1996-1073

www.mdpi.com/journal/energies

Article

RETRACTED: Optimization and Characterization of Lithium Ion Cathode Materials in the System $(1 - x - y)LiNi_{0.8}Co_{0.2}O_2 \bullet xLi_2MnO_3 \bullet yLiCoO_2$

Venkatesan Manivannan *, Madhu Chennabasappa and Joshua Garrett

Department of Mechanical Engineering, Colorado State University, Fort Collins, CO 80523, USA; E-Mails: chanabasappa.madhu@gmail.com (M.C.); joshgarrett@gmail.com (J.G.)

* Author to whom correspondence should be addressed; E-Mail: mani@engr.colostate.edu; Tel: +1-970-491-2207; Fax: +1-970-491-3827.

Received: 17 February 2010 / Accepted: 1 April 2010 / Published: 21 April 2010

Abstract: There is ongoing effort to identify novel materials that have performance better than $LiCoO_2$. The objective of this work is to explore materials in the system $(1 - x - y)\ LiNi_{0.8}Co_{0.2}O_2 \bullet xLi_2MnO_3 \bullet yLiCoO_2$. A ternary composition diagram was used to identify sample points, and compositions for testing were initially chosen. Detailed characterization of the synthesized materials was done, including Rietveld Refinement of XRD data, XPS analysis for valence state of transition-metals, SEM for microstructure details, and TGA for thermal stability of the materials. Electrochemical performance showed that discharge capacities on the order of 230 mAh/g were obtained. Preliminary results showed that these materials exhibit good cycling capabilities thereby positioning these materials as promising for Li-ion battery applications.

Keywords: Li-ion battery; battery efficiency; battery life; cycle life

RETRACTED

1. Introduction

Pioneering effort by Goodenough in the field of Li-ion battery cathode materials has positioned Li-ion battery technology as a viable technology for portable electronic applications and, more recently, for transport applications, after the proof of concept demonstration (reversible insertion/extraction of lithium from layered TiS_2) [1–8]. Accordingly, $LiCoO_2$, $LiNiO_2$, and $LiMn_2O_4$ materials were explored initially as cathode materials for Li-ion battery technology. Extensive R&D work has allowed successful implementation of $LiCoO_2$ batteries by Sony in the early 1990's [9]. The structural instability, high cost, and non-environmental friendliness of cobalt materials make

exploration of $LiNiO_2$ materials attractive for Li-ion batteries [10]. However, the cation ordering associated with $LiNiO_2$ has prevented the full realization of this electrode material [11–13]. This led to the investigation of solid solution between $LiNiO_2$ and $LiCoO_2$ with other dopants such as Fe and Al, resulting in material systems such as $LiNi_{1-y}Co_yO_2$, $Li_xFe_yNi_{1-y}O_2$, and $LiAl_{1/4}Ni_{3/4}O_2$. [14–16]. Two-dimensional layered materials based on Mn were explored by Peter Bruce *et al*. [17]. Additional improvements in the layered insertion materials were proposed by Ohzuku *et al*. for cathode materials with composition $LiNi_{0.5}Mn_{0.5}O_2$ [18], in addition to the investigation of the system $Li_x(Mn_yNi_{1-y})_{2-x}O_2$ by Bates [19]. Ohzuku reported novel $LiMn_{1/3}Ni_{1/3}Co_{1/3}O_2$ which was investigated further [20]. Significant contributions were made in improving the layered two-dimensional materials by the Ohzuku, Dahn, Kanno, Zhecheva and Stoyanova groups [21,22].

Stoyanova *et al*. reported the effect of manganese substitution for cobalt in solid solution ($LiCoO_2$-$LiMnO_2$), which led to the development of composite-type cathodes [23]. Solid solutions between $LiMO_2$ (M = Cr) and Li_2MnO_3-layered materials with superior electrochemical performance were demonstrated by Dahn and other groups [24]. A new series of material with the general formula $xLi_2MO_3 \bullet (1 - x)LiMn_{0.5}Ni_{0.5}O_2$ (M = Ti, Mn, Zr) for x = 0 to 0.3 was reported [25]. Approaches to prevent the conversion of layered $LiMnO_2$ to spinel were explored which led to subsequent improvements of the material [26]. Layered compositions representing solid solution between Li_2MnO_3, *i.e.*, $Li[Li_{1/3}Mn_{2/3}]O_2$ and $LiMn_{0.5}Ni_{0.5}O_2$, were shown to exhibit high capacities [27]. The new series of cathodes representing a solid solution between layered $Li_2MnO_3 \bullet Li[Li_{1-x}Mn_{(2-x)/3}Ni_{x/3}Co_{x/3}]O_2$ was proposed by Manthiram *et al*. which resulted in a high capacity of 285 mAh/g with low irreversible capacity loss [28]. These studies show that new cathode materials based on structural investigation are possible among several sub-classes of layered materials such as $LiCoO_2$, $LiNi_{0.5}Co_{0.5}O_2$, $LiNi_{1/3}Co_{1/3}Mn_{1/3}O_2$, and combinations thereof. Insertion materials such as $LiCo_{1-2x}Ni_xMn_xO_2$ (which is a solid solution of $LiCoO_2$ and $LiNi_{0.5}Mn_{0.5}O_2$) and $Li[Ni_xLi_{1/3-2x/3}Mn_{2/3-x/3}]O_2$ (a solid solution of $LiNi_{1/2}Mn_{1/2}O_2$ and Li_2MnO_3) can exhibit satisfactory performance. However, when charged to 4.8 V, due to simultaneous removal of Li^+ and O^{2-}, these materials resulted in high initial irreversible capacity losses, potentially leading to safety concerns [29,30].

Zhang *et al*. reported novel cathode materials by developing solid solutions between three layered compounds: $LiNi_{1/2}Mn_{1/2}O_2$, $LiCoO_2$, and Li_2MnO_3 (*i.e.*, $Li[Li_{1/3}Mn_{2/3}]O_2$). The materials belonging to this composition diagram were synthesized by conventional solid state reactions [31]. The points chosen were concentrated in the high $LiNi_{1/2}Mn_{1/2}O_2$ content region of the composition diagram (top region of the diagram), and cells were cycled between 4.4 or 4.6 V, to 2.5 V. Samples tested at the higher charge voltage showed that increasing the $Li[Li_{2/3}Mn_{2/3}]O_2$ content led to increased capacity and better cyclability, but also had increased irreversible capacity loss (ICL), whereas the $LiCoO_2$ component primarily contributed to increased capacity accompanied by fading during cycling. $LiNi_{0.8}Co_{0.2}O_2$ (~190 mAh/g) materials have been reported to have higher capacities than $LiNi_{1/2}Mn_{1/2}O_2$ (~150 mAh/g) [18]. We envisaged that by replacing one of the end-members, $LiNi_{1/2}Mn_{1/2}O_2$, with $LiNi_{0.8}Co_{0.2}O_2$, better capacities than reported could be achieved. Therefore the objectives of our work are (a) build a ternary compositional diagram with $LiNi_{0.8}Co_{0.2}O_2$ as one of the end members while retaining $LiCoO_2$ and Li_2MnO_3 (*i.e.*, $Li[Li_{1/3}Mn_{2/3}]O_2$) at corners, and (b) choose select compositions that are spread over the entire region of the ternary diagram that also give good representation of the compositional space. Applying this approach would ensure that the select

RETRACTED

compositions integrated both Li_2MnO_3 (*i.e.*, $Li[Li_{1/3}Mn_{2/3}]O_2$) and $LiCoO_2$ at high content levels and a "sweet spot" composition could be found that has better performance than reported. The material synthesis conditions were kept the same as that of Zhang *et al*. to retain the less-complex solid-state synthesis and minimize the effect of varying synthesis procedures.

2. Results and Discussion

2.1. Structural studies

The ideal replacement of the $LiNi_{1/2}Mn_{1/2}O_2$ end member in the ternary diagram would be $LiNiO_2$ as an end member. However, we found that the synthesis conditions employed (*i.e.*, 975 °C, 4 hours, liquid nitrogen quench) have resulted in NiO formation only, and accordingly we have chosen $LiNi_{0.8}Co_{0.2}O_2$ as a corner of the compositional diagram (Figure 1). It is known that introduction of small amounts of Co stabilizes the $LiNiO_2$ structure, leading to high specific capacities [16]. Choosing this composition has now provided the advantage that a common synthesis condition be applicable to all the compositions of the ternary diagram (see Table 1 for compositions of materials chosen). This is indeed the case that the XRD showed the synthesized compounds are single-phase in nature (Figure 2).

Figure 1. Compositional ternary diagram representing regions of materials studied.

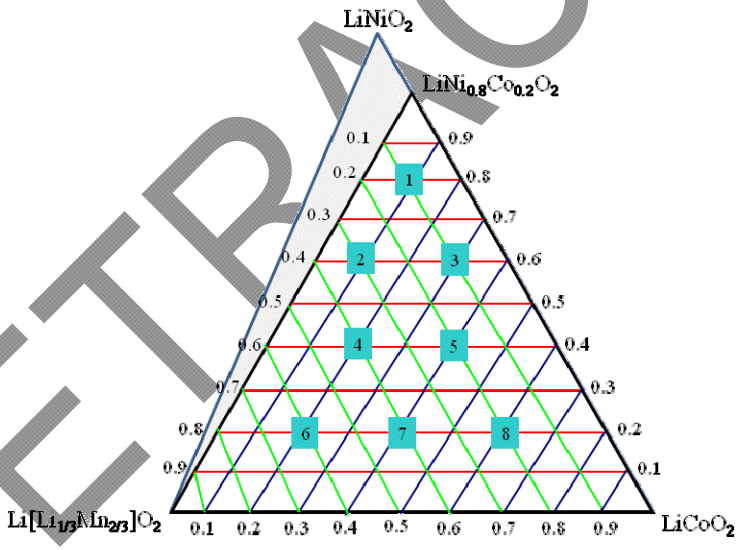

The powder X-ray diffraction of these eight compositions is given in Figure 2. X-ray diffraction patterns showed that all the compositions crystallize in a R-3m space group and belong to the two-dimensional layered Li[Ni, Co]O_2 class of materials. In comparison to JCPDF standard, X-ray diffraction patterns were indexed with lattice parameters $a \sim 2.84$ Å, and $c \sim 14.1$ Å [32]. The crystal structure details of all the compositions are presented in Table 1. Also it was shown that the intensity ratio of (0 0 3) and (1 0 4) peaks is an indication of degree of cation ordering of $LiNiO_2$, and a value of <1.2 could lead to poor electrochemical performance [33]. We have calculated that the intensity ratios of the materials are 0.69, 1.22, 1.21, 0.90, 1.19, 1.29, 1.12, and 1.07 respectively for samples #1 to # 8. It is noteworthy that the best performing materials (such as sample 6) have values greater

RETRACTED

than 1.2. ICP-AES analysis of best compositions was performed, and the compositions calculated based on the ratio of the concentrations are in agreement with the synthesized compositions within the limits of error (Table 1).

The synthesized materials belong to layered compounds of α-$NaFeO_2$ type which is considered of distorted type (FCC array distorted along the hexagonal *c*-axis). This distortion is reflected in the XRD patterns, and accordingly the peaks around 2θ = 37 split into (006, 102) and peaks close to 70 split into (108, 110) Miller indices. When the distortion is absent, the splitting of the peak will not appear and merge into a single peak (the structure is cubic with extreme case of cation mixing). Therefore the value of *c/a* ratio is evidence of the degree of ordering of the layered structure as well as the amount of transition metal in the inter-slab structure. For *c/a* ratios greater than $\sqrt{24}$ = 4.899, it is reasonable to expect that the layered structure is formed, overcoming the distortion of oxygen lattice. It is indeed the case in our samples, the calculated *c/a* ratio values are 4.933, 4.943, 4.942, 4.949, 4.943, 4.974, 4.989, and 4.937 respectively for samples #1 to #8 [34]. In order to determine the cationic distribution and thereby the crystal structure more accurately, detailed Rietveld refinement of the structural analysis was performed.

Figure 2. Powder XRD patterns of samples of the $(1 - x - y)LiNi_{0.8}Co_{0.2}O_2 \bullet xLi_2MnO_3 \bullet yLiCoO_2$ system of compositions, marked from #1 to # 8, whose compositions are given in Table 1.

RETRACTED

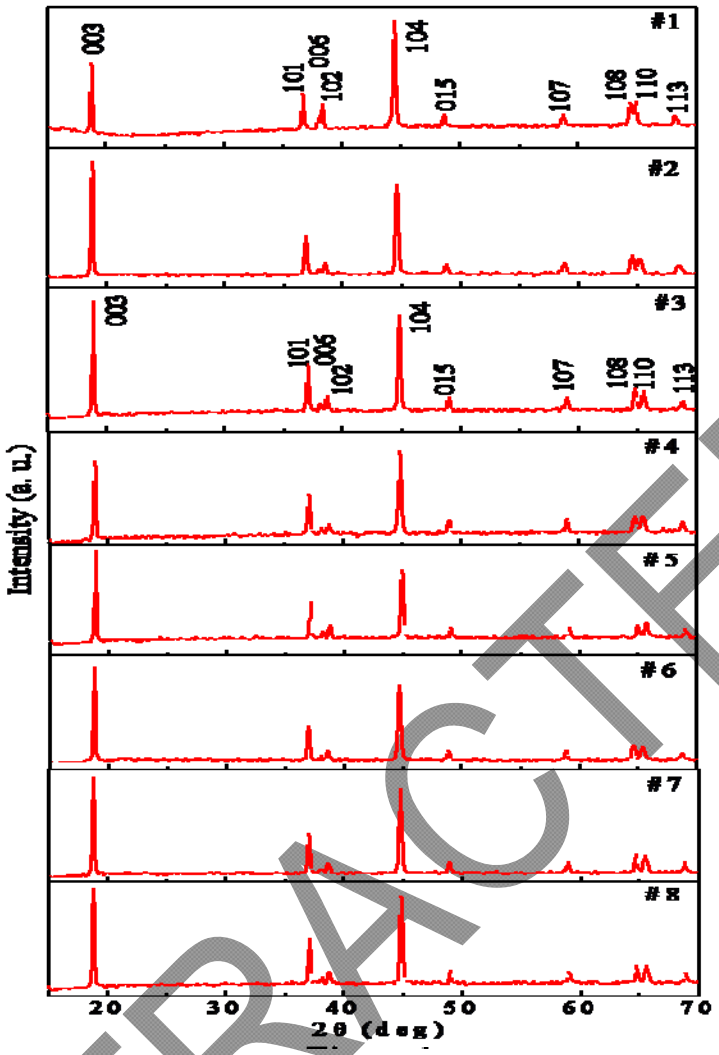

Table 1. Compositions, crystal structure, and electrochemical results of (1 – x – y) $LiNi_{0.8}Co_{0.2}O_2$ • $xLi[Li_{1/3}Mn_{2/3}]O_2$ • $yLiCoO_2$.

	Compositions	Space Group	*a* Å	*c* Å	Discharge capacity (mAh/g) 4.6–3 V	4.6–2.75 V	4.6–2.5 V	4.6–2 V
#1	$Li_{1.033}Mn_{0.067}Ni_{0.64}Co_{0.26}O_2$	R-3m	2.883(2)	14.222(3)	118	122	128	141
#2	$Li_{1.1}Mn_{0.200}Ni_{0.48}Co_{0.22}O_2$		2.869(5)	14.182(1)	186	192	198	209
#3	$Li_{1.033}Mn_{0.067}Ni_{0.48}Co_{0.42}O_2$ *		2.857(1)	14.119(5)	177	184	190	216
#4	$Li_{1.133}Mn_{0.267}Ni_{0.32}Co_{0.28}O_2$		2.853(2)	14.119(3)	172	177	182	191
#5	$Li_{1.067}Mn_{0.133}Ni_{0.32}Co_{0.48}O_2$		2.848(6)	14.080(2)	177	183	189	199
#6	$Li_{1.2}Mn_{0.4}Ni_{0.16}Co_{0.24}O_2$ *		2.842(3)	14.136(2)	190	203	215	230
#7	$Li_{1.133}Mn_{0.267}Ni_{0.16}Co_{0.44}O_2$		2.85(1)	14.220(4)	166	175	185	199
#8	$Li_{1.067}Mn_{0.133}Ni_{0.16}Co_{0.64}O_2$		2.856(2)	14.101(1)	164	171	179	192

* Formula as per ICP-AES are $Li_{1.02}Mn_{0.06}Ni_{0.51}Co_{0.39}O_2$ (sample #3) and $Li_{1.18}Mn_{0.39}Ni_{0.15}Co_{0.26}O_2$ (sample #6).

2.2. Rietveld structural refinement details

RETRACTED

Two dimensional layered $LiNiO_2$ materials are known to display cation disordering (*i.e.*, a contrary to standard R-3m group where Li occupies the 3a position, Ni in the 3b, and O in the 6c position; the cation ordering results in some amount of Ni in 3a sites). This cation disorder ($Li_{1-z}Ni_{1+z}O_2$) was attributed to poor cycling performance of $LiNiO_2$ material [33]. In order to understand the role of the different transition metals in this series, detailed Rietveld refinement was performed. Applying the oxidation state and ionic radius, a model for cationic distribution is derived. Considering the ionic radii of Ni^{3+} (0.56 Å), Ni^{2+} (0.70 Å) to that of Li^+ (0.74 Å), Ni entering Li would be divalent in nature. Neutron diffraction experiments on $LiNi_{1-y}Co_yO_2$ showed that Co ions do not exist at the 3a Li site (as Co^{3+}) [35]. The Rietveld refinement of $Li[Ni_xLi_{1/3-2x/3}Mn_{2/3-x/3}]O_2$ by Dahn *et al*. has shown that a model with Mn atoms moving to the Li-layer has given a good fit initially for structural refinement for the XRD data [27]. However, neutron diffraction that was applied to identify the disordering of Ni and Mn atoms showed an excellent fit to the model when Ni atoms occupy positions in the Li layers. In addition, a model with Mn atoms moving into Li layers resulted in unphysical values for the site occupations. Accordingly, we decided to refine our data with the following models: (a) Mn atoms in Li layers and (b) Ni atoms in Li layers. The long-scan data showed that around $2\theta = 20°$, additional Bragg reflections were present. These were attributed to superlattice reflections due to ordering of Li and Mn atoms which reduces the symmetry from R-3m to C2/m, and these were accordingly taken into consideration during refinement. In both cases we have employed a two-phase approach to refine the XRD data (*i.e.*, R-3m with C 2/m, to account for superlattice reflections). The best fit for our data is obtained for model b—*i.e.*, Ni atoms present in Li layers. The Rietveld refinement results of both the models are presented in Figure 3. Rietveld results in conjunction with ionic radii showed a general formula of the cationic distribution for the materials: $[Li_{1-z}M_z{}^{2+}]_{3a}$ $[M^{3+}{}_{1-z-2y}M^{2+}{}_{y+z}Mn^{4+}{}_y]_{3b}[O_2]_{6c}$, which would also account for charge compensation at the 3b site.

Figure 3. Rietveld refinement results of composition # 6 using different models.

RETRACTED

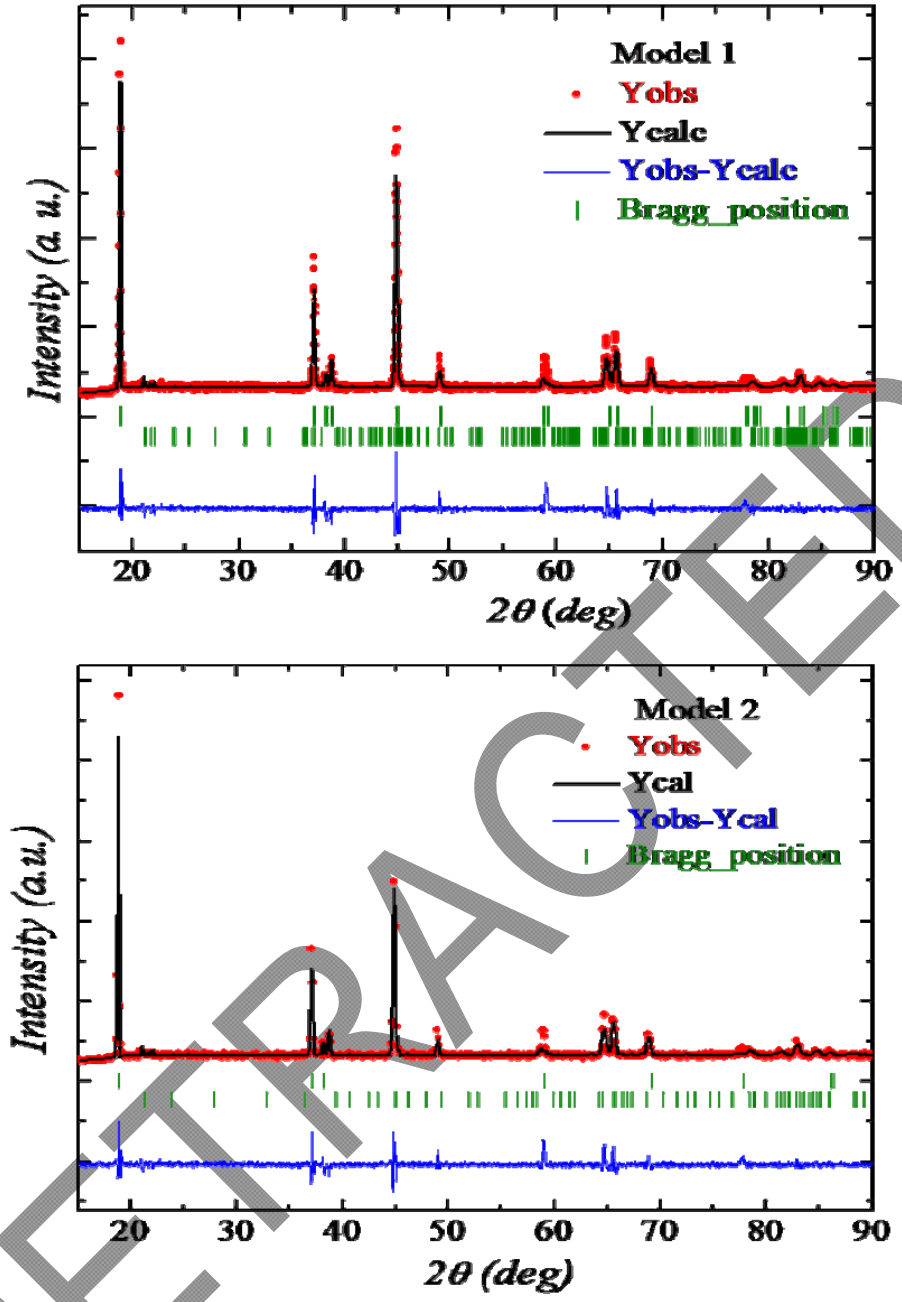

RETRACTED

Table 2 gives crystal structural details as a result of the Rietveld refinement. The results of structural refinement are analyzed using CrystalMaker^{R} software [36] to obtain the crystal structure diagrams (Figure 4), from which the relevant bond lengths and angles between metal-oxygen coordination were derived (Table 2) [36, 29].

Table 2 showed the amount of transition metals at the 3a Li site for both the models (up to 1.7%). In addition, the data on interatomic distances also supported the "cationic distribution" model. The M-O bond lengths obtained are 2.012 Å, and 2.013 Å respectively in case of M = Mn and Ni respectively. The bond length of Co-O with low-spin Co^{3+} is 1.945 Å, and with high-spin Co^{2+} is 2.01 Å. Similarly the bond length of Ni-O with low spin Ni^{3+} is 1.96 Å, and high-spin Ni^{2+} is 2.01 Å [33]. Our bond-length results in comparison are suggestive that Ni^{2+} and or Co^{2+} are present at 3a site (Co^{3+} cannot be present per neutron diffraction studies) and Co^{3+}, Mn^{4+} present at the 3b site. The redox

changes associated with such transition-metals plays an important role in determining the electrochemical properties of the materials.

Table 2. Rietveld refinement results of composition #6.

	Lattice parameter (Å)	z(O)	Li_{3a}	Occupancy of M in Li layer	χ2	R_{wp} (%)	R_B (%)	Bond Length(Å)	Bond Angle(°)
Model 1	*a* = 2.842(2) *c* = 14.136(7)	0.249(1)	0.988	z(Mn) 0.015	1.15	7.95	15.8	*Mn-O* 2.012 *Li-O* 2.029	*O-Mn-O* 90.11 *O-Li-O* 88.96
Model 2	*a* = 2.842(2) *c* = 14.136(7)	0.247(3)	0.982	z(Ni) 0.017	1.21	8.10	12.6	*Ni-O* 2.013 *Li-O* 2.027	*O-Ni-O* 89.79 *O-Li-O* 89.05

Figure 4. Crystal structures of composition #6 created with CrystalMaker software.

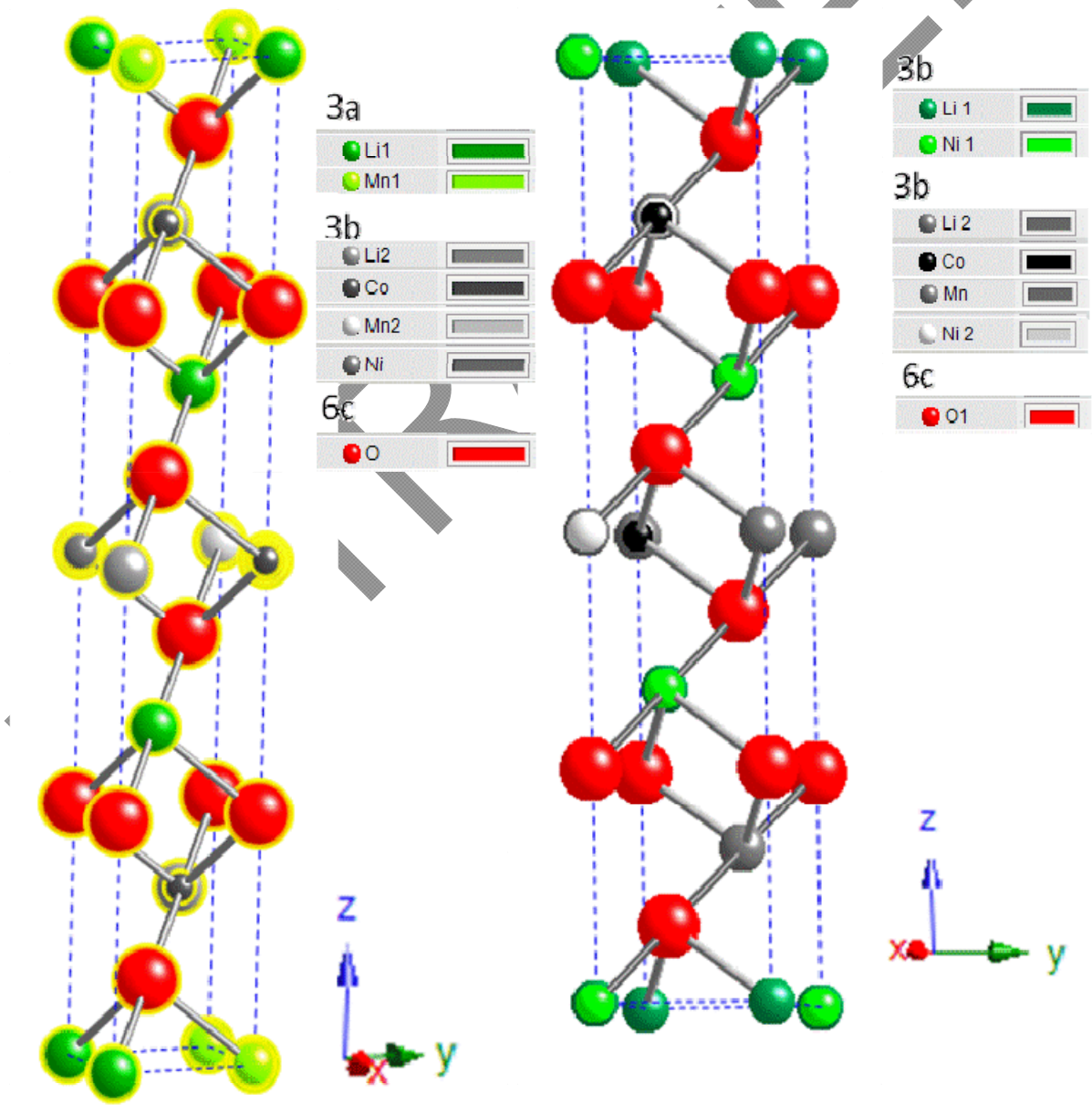

2.3. Microstructural studies

TGA was performed to evaluate the thermal stability of the material (Figure5). Within the temperature range of study, the samples lose a small percentage of weight continuously (total 3%). Weight loss up to 300 °C (about 2.5 wt %) could be due to loss of water molecules [38]. The small weight loss (~0.5 wt %) up to 600 °C indicates there was so significant loss corresponding to the material and the material is stable. TGA of $LiNiO_2$ showed that there was negligible weight loss up to 860°C followed by decomposition of $LiNiO_2$ to $Li_{1-x}Ni_{1+x}O_2$ along with oxygen evolution [39]. TGA results of our samples showed that they are thermally stable within the testing range (our instrument had limited testing range). Figure 6 shows the SEM images of all the compositions synthesized. SEM showed that the oxide particles have controlled morphology, generally are submicron in size, and have homogeneous distribution. Also the particles are interconnected well, which would facilitate good transport properties.

Figure 5. TGA of synthesized materials.

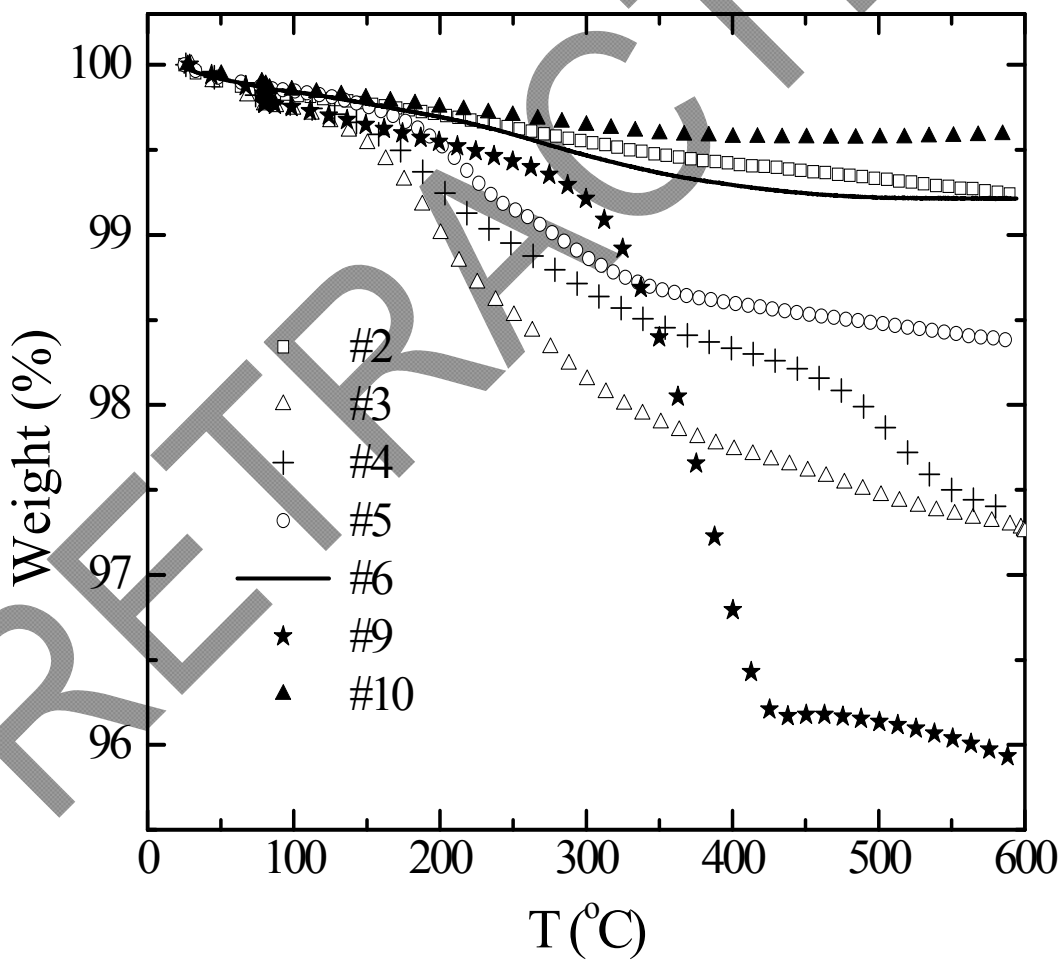

RETRACTED

Figure 6. SEM images of synthesized materials. All images are taken at 5000 magnification and the scale bar represents 1 μm.

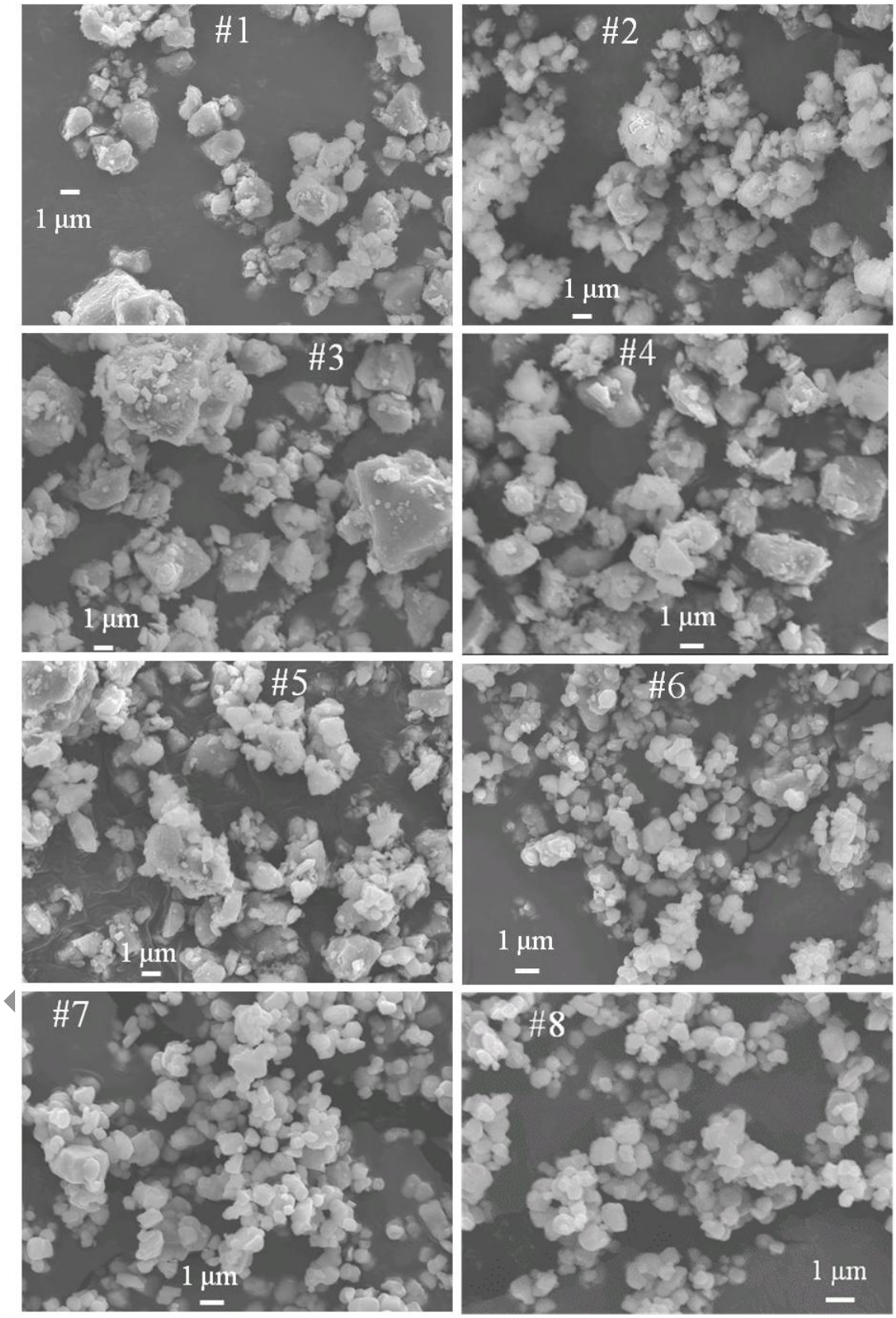

2.4. XPS Studies

X-ray photoelectron spectroscopy (XPS) is a well established, non-destructive technique for evaluation of valence states of the metals/ions in solids and is extensively applied in the characterization of cathode materials [34]. We have applied this technique to determine the valence states of our cathode materials synthesized. The valence states of the transition metals provide an idea of the redox couples associated with the intercalation process of lithium.

The measurement was done on uncharged samples at room temperature to determine the valence states of transition metals such as Ni, Mn and Co by obtaining a full-scan spectrum (up to 1200 eV) which contains signatures of valence states of the elements. The binding energy of C1s peak at 248.8 eV was used as the reference [40]. In order to analyze and meet the objectives, the spectral data of each sample is split into regions of interest and such results are presented in Figure 7. For example, in Figure 7, #1 gives a spectral response corresponding to Ni, Co, Mn, and O atoms corresponding to the composition #1, by splitting into regions around 850, 780, 640, and 530 eV, respectively.

For sample #1, the binding energy of Ni, Ni2p$_{3/2}$ showed an asymmetric peak in addition to the satellite peak (Figure 7a). The overall spectrum is deconvoluted into two Gaussian peaks, The binding energy of the main peak is at 854 eV, which is indicative of Ni in the 2+ valence state and compares with other Ni^{2+}, containing compounds, such as NiO. The peak situated at higher energy (856 eV) corresponds to Ni^{3+}, as observed in Ni^{3+} containing compounds such as $LiNiO_2$. The shift indicates an increase in the positive interaction between the electrons of 2p$_{3/2}$ and the nucleus increases resulting in higher energy needed to pull the electron from Ni^{3+} level (Ni^{3+} has fewer electrons). The satellite peak at 860 eV is attributed to the multiple splitting in the energy levels of the Ni-containing oxides such as NiO or $LiNiO_2$. The XPS results showed that the predominant state of Ni in the synthesized material is 2+ [41].

Figure 7b shows the binding energy corresponding to Li 1s core levels in the region 52–56 eV. The fitting and deconvolution of Li (1s) spectrum gives the major peak binding energy at 54.5 eV, which is similar to lithium in an octahedral environment of oxygen atoms, such as in $LiCoO_2$ [41]. Figure 7c shows the O 1s spectrum, which has a main peak around 529 eV and another peak at 533 eV that can be deconvoluted to three individual contributions [34,42]. The peak at 529 eV can be assigned to O^{2-} ions, and the shoulder peak could represent a degree of oxidation more than O^{2-} due to transition metal-oxygen covalent bonds. Accordingly, the binding energies observed at 529 eV, 531.3 eV, and 532.4 eV could be assigned as contributions from the Mn-O, Co-O, and Ni-O bonds, respectively, implying the influence of the covalent nature of their bonds [34]. The distribution of transition metal atoms contributed to the strong superlattice reflections as seen in the XRD patterns. The ordering of Li and transition metal atoms in the rock salt structure of the compound has a transition metal layer consisting of Ni^{2+}, Mn^{4+}, and Co^{3+}, separated by Li^{+} layers, and the vertices of the hexagon occupied by Mn^{4+} and Co^{3+}, with Ni^{2+} in the center. The ordering has resulted in reducing the symmetry from R-3m to C2/m.

Figure7d shows the Co 2p core level spectra which show Co 2p$_{3/2}$ peaks in the 778–782 eV range and Co 2p$_{1/2}$ peaks in the 792–797 eV range. The spectrum also has weak satellite peaks. The Co 2p$_{3/2}$ peak was fit into a single peak with the binding energy of 779.9 eV which matches with the binding

RETRACTED

energy reported for Co^{3+} in $LiCoO_2$. The binding energy of Co is indicative of Co^{3+} in low spin configuration. The peak at 796 eV corresponding to Co $2p_{1/2}$ is assigned to high spin Co^{2+} ions [43].

The XPS spectrum in Mn 2p core levels is shown in Figure 7e, in which the 3/2 and 1/2 orbit doublet components are seen at 642 eV and 655 eV, respectively. The asymmetric nature of the spectrum suggested deconvolution of the spectrum to identify the major peak position which would indicate the predomoninant state of Mn. The deconvolution resulted in two binding energies for the best fit. The major peak centered at 642.5 eV, which in comparison with the binding energies of Mn, containing compounds such as MnO_2 (major peak at 642.5 eV) and Mn_2O_3 (641.8 eV), strongly suggested the 4+ valence of Mn and accordingly, the value was assigned. The secondary peak is attributed to the energy level splitting of Mn $2p_{3/2}$ electronic levels [44]. Thus the predominant valence states of transition metals in our samples were determined to be Ni^{2+}, Co^{3+}, and Mn^{4+}, respectively. It is to be noted that in the well-known oxide cathodes, like $LiNiO_2$, Li (Ni, Co)O_2, and Li(Mn, Co)O_2, with the α-$NaFeO_2$ structure, the metals Ni, Mn, and Co are only in a 3+ oxidation state [33].

XPS study was extended to other synthesized materials and the results are presented in Table 3. The binding energy peak positions of lithium, cobalt, nickel, and manganese are evidenced in the XPS spectra. The binding energy of lithium is at ~55 eV indicating that the lithium atoms are in an octahedral environment. The oxygen O (1s) core level was observed at 530.5 eV. The binding energy peaks of Co ($2p_{3/2}$) and Co ($2p_{1/2}$) are observed at ~779 eV and ~795 eV, respectively, attributing to the Co^{3+} bonding states of these materials in a possible octahedral arrangement. The Ni 2p XPS spectrum is indicative of the charge—transfer nature of an octahedral 2+ metal ion; however, the broad and splitting nature ($2p_{3/2}$, $2p_{½}$) is suggestive of a valence state of Ni greater than +2. The binding energy separation of about 15 eV is in good agreement with previous results. The Ni $2p_{½}$ and $2p_{3/2}$ spectra are observed at ~875 eV and ~857 eV, respectively, with a binding energy separation of about ~17 eV. Most of the compounds showed Mn $2p_{½}$ to Mn $2p_{3/2}$ peak separation at ~11 eV. The summary of XPS results showed that the predominant oxidation states of Ni, Co, and Mn are +2, +3, and +4 respectively [45]. This result implies that the primary redox couples involved in the electrochemical process will be Ni^{2+}/Ni^{4+} and Co^{3+}/Co^{4+} as the Mn^{4+} ion does not oxidize in the voltage window used.

Table 3. Summary of XPS results of the compositions investigated.

Sample	$Mn2p_{1/2}$	$Mn2p_{3/2}$	ΔMn	$Ni2p_{1/2}$	$Ni2p_{3/2}$	ΔNi	$Co2p_{1/2}$	$Co2p_{3/2}$	ΔCo
#1	-	642.8	-	871.6	854	17.6	794.0	778.9	15.1
#2	-	642.0	-	871.6	854.8	16.8	794.0	779.6	14.4
#3	-	642.0	-	871.6	854.8	16.8	794.8	779.6	15.2
#4	653.2	642.8	10.4	870.8	854.0	16.8	794.0	778.8	15.2
#5	653.2	642.0	11.2	870.8	854.0	16.8	794.0	778.8	15.2
#6	652.4	642.0	10.4	870.1	853.2	16.9	794.0	778.8	15.2
#8	652.4	641.2	11.2	869.8	853.3	16.5	793.2	778.0	15.2

RETRACTED

Figure 7. XPS spectra of all the compositions showing the electronic transitions of elements present. Measured and fitted transition-metal spectra of the # 6. (□) represents the measured data points, (closed symbols) individual curve, (- -) Shirley background, and (-) summation curve. Peak assignments are discussed in the text.

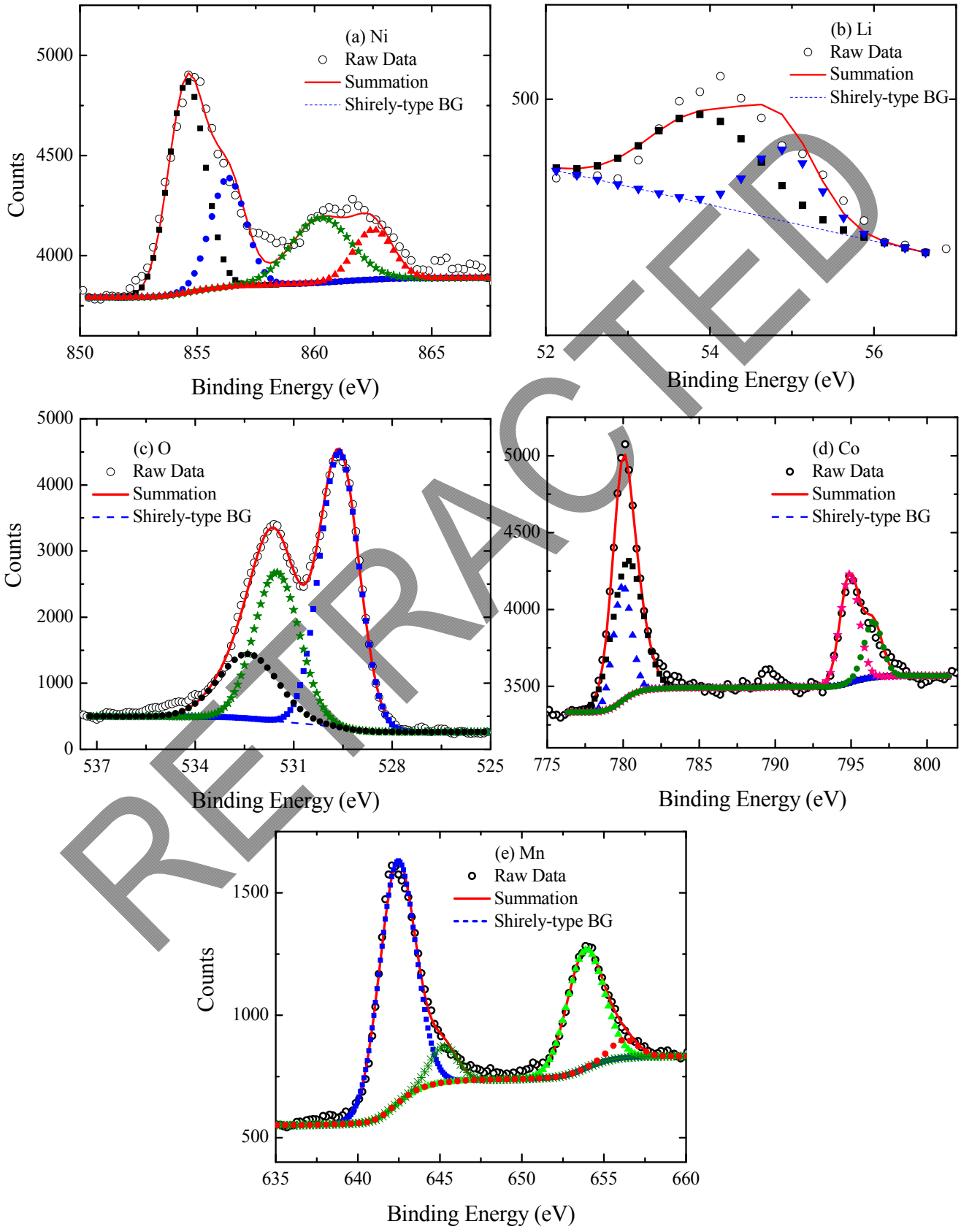

RETRACTED

2.5. Electrochemical results

The electrochemical performances of all compositions in the voltage range 4.6 to 2 V are presented in Figure 8. The system showed fairly consistent charge/discharge curves throughout the composition range, and the discharge capacities varied between 140 and 230 mAh/g in the voltage range of 4.6 to 2 V. The discharge capacities of these compositions are presented in Table 1. The discharge profiles were nearly flat with a mid V_{oc} of approximately 3.8 eV. Sample #6 showed a long gradual drop resulting in the highest capacity when discharged to 2V.

2.6. Discussion

In general, the materials showed discharge capacities in the 140–230 mAh/g range (Table 2). We have looked at the specific capacity of the materials by dividing the overall capacity plot into four regions: 4.6–3 V, 4.6–2.75 V, 4.6–2.5 V, and 4.6–2 V, to comment on the usefulness of these materials for applications. The results are presented in Table 2. In the 4.6–3 V region, the best capacity is obtained for sample # 6 (190 mAh/g). Also sample #2 has nearly the same capacity at the 3 V level which is often taken as the cutoff of a practical cycle. When the range is extended to 2.75 V, sample #6 provides >200 mAh/g capacity, with sample #2 closely (>190 mAh/g). At the 2 V range there are four materials that have capacities >200 mAh/g. It is noteworthy that sample #6 has the highest discharge capacity at every charge level with the highest reproduced results of 230 mAh/g. The discharge profiles of the compositions, as shown in Figure 9a, exhibited a nearly flat, but clearly sloping pattern. Also the preliminary cyclability tests as shown in Figure 9b exhibit good capacity retention for the best composition under testing conditions (composition # 6).

The redox processes associated in the electrochemical process are derived from the charge/discharge curves. During the charging process, Li^+ extraction occurs during charging from 3.4 V to about 4.4 V with concomitant oxidation of Ni^{2+} and Co^{3+}, but around 4.5 V involves electrochemical activation of Li_2MnO_3 resulting in irreversible lithium and oxygen removal in the form of Li_2O and MnO_2 ($Li_2MnO_3 \rightarrow MnO_2 + Li_2O$). During the discharge, lithium insertion takes place at about 4.3 V, with a smooth sloping profile (with a mid V_{oc} at about 3.8 V of the discharge curve) that could correspond to reducing Ni^{4+}/Ni^{2+} electrochemical redox couple and Co^{4+} reducing to Co^{3+}, and then into a layered MnO_2 component below 3.5 V down to 2 V (with a Mn^{4+}/Mn^{3+} redox couple). This has resulted in gradual insertion of Li into the layered structure and the extended discharge profile has a specific capacity of about 230 mAh/g.

Results showed that the best composition, #6, with composition $Li_{1.2}Mn_{0.4}Ni_{0.16}Co_{0.24}O_2$, in the range 4.6–2.5 V, had a discharge capacity of 215 mAh/g compared to ~200 mAh/g for $Li_{1.133}Mn_{0.517}Ni_{0.250}Co_{0.100}O_2$, which was the highest capacity in Zhang's results [31]. The results showed the effect of integrating Li_2MnO_3 (*i.e.*, $Li[Li_{1/3}Mn_{2/3}]O_2$) and $LiCoO_2$ into the structure as well as optimizing the regions of high manganese and cobalt content. This approach has helped to identify materials with high capacity. It is noteworthy that sample #6 corresponding to 60% Li_2MnO_3 content had an ICL of ~60 mAh/g (in comparison to projected higher ICL of Zhang's results by extrapolation at the same Li_2MnO_3 content).

RETRACTED

It is noteworthy to mention that sample #6 had the highest Mn content (0.4 *vs.* 0.27 for the next highest #7). Integrating 2-D layered Li_2MnO_3 into isostructural components has indeed resulted in improved performance. It is known that when charging Li_2MnO_3 to 4.5 V, only 20 mAh/g can be extracted [46], but on charging to 5.0 V a capacity of 383 mAh/g (83% of the material's theoretical capacity) can be achieved. This increased capacity is due to the electrochemical extraction of Li and the chemical extraction of oxygen that occurs at potentials >4.5 V [25a]. Therefore, charging sample #6 beyond 4.5 V to 4.6 V has helped to get additional charge capacity. The charging to 4.6 V does not result in complete removal of oxygen from the structure, allowing some amount of lithium to be utilized during the intercalation process. This helps to maintain good cyclability of the material, but also results in some ICL. Efforts are in progress to look at compositions around the most promising compositions of this system with high Mn content and utilizing modified synthesis procedures that help to obtain a high capacity material that is cost-effective and has lower ICL.

Figure 8. Electrochemical testing of all the compositions showing the first charge and discharge curves at 0.1 mA/cm^2.

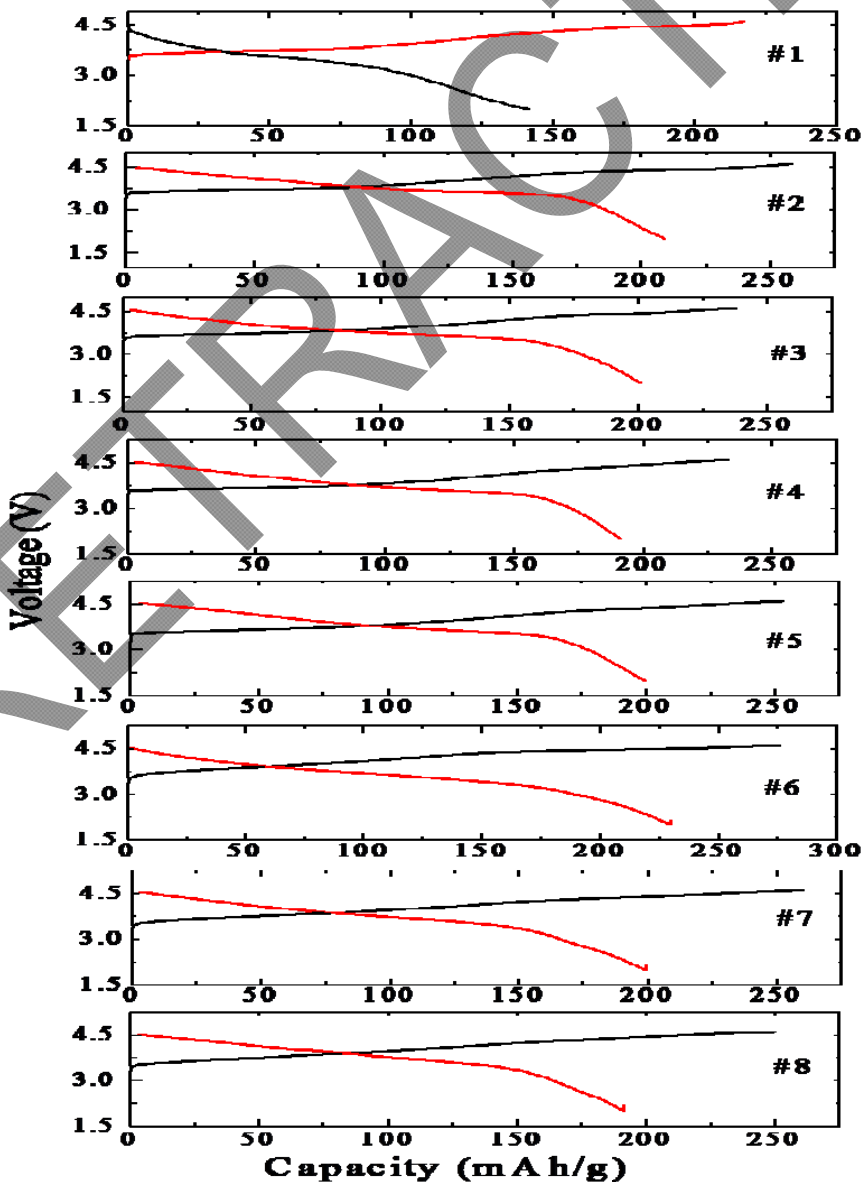

RETRACTED

Figure 9. (a) Discharge voltage profiles of all the compositions. (b) preliminary extended life-cycle testing of the materials.

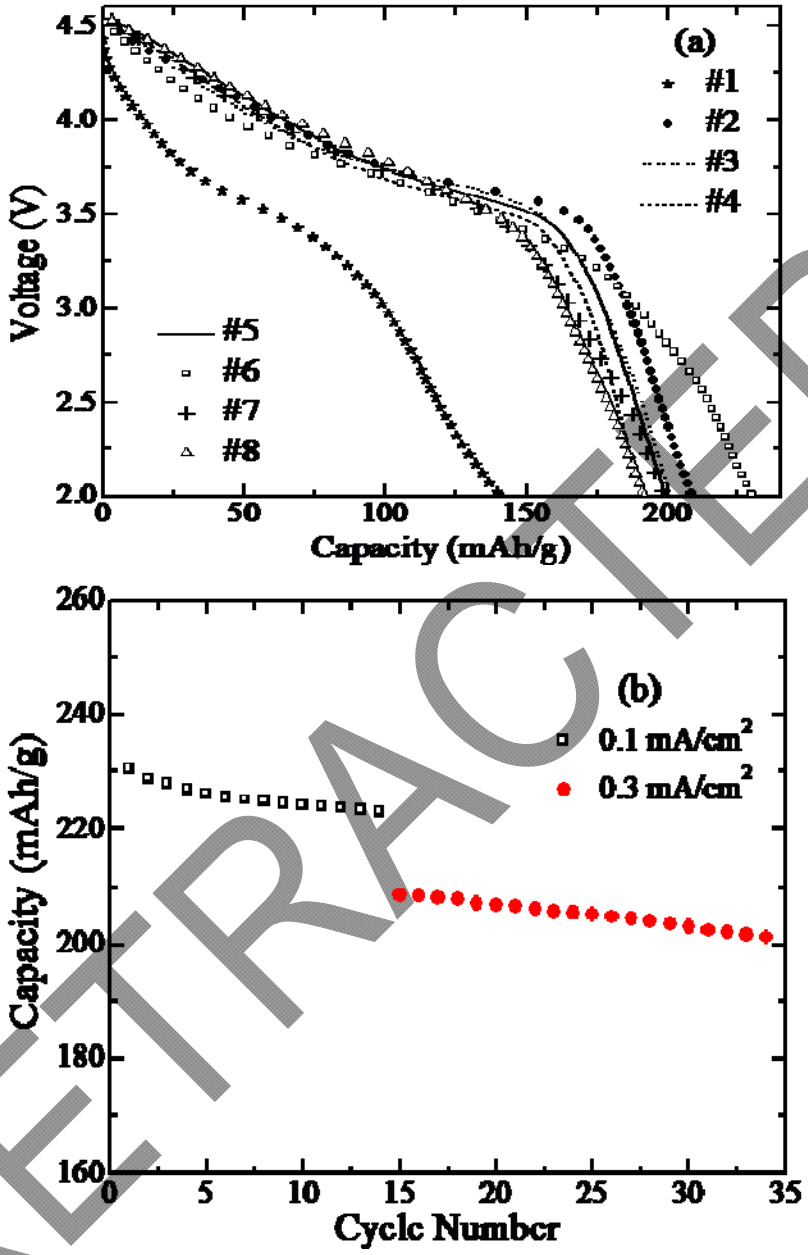

RETRACTED

3. Experimental Section

3.1. Synthesis

All the compositions of the system were synthesized by conventional solid state reactions. Accordingly, stoichiometric quantities of the required precursors (lithium acetate, manganese acetate, nickel acetate, and cobalt acetate) were thoroughly mixed using mortar and pestle, and the powders were subjected to an initial heating at 450 °C for 8 hours to convert the precursors to basic oxides. Then the powders were ground, pelletized, and subjected to a second heating at 975 °C for 4 hours before quenching in liquid nitrogen.

3.2. Characterization

The phase purity and crystal structure details were examined by Scintag X-ray diffraction using Cu-K_α radiation. For Rietveld refinement, data were collected at a scan rate of 0.5°/min, with a step size of 0.2° in 2θ, over a range of 10° to 90°. The data were refined using the Rietveld analysis program FullProf [47,48]. The morphology of the powder was examined using a JEOL JSM-840A SEM, a field emission system with the in-lens thermal field emission electron gun. Elemental analysis of the compositions was performed by the ICP-AES method (Jarrell-Ash dual view, high resolution IRIS Advantage inductively coupled plasma). Thermogravimetric analysis (TGA) was performed using a weight and temperature-calibrated TA Instrument 2160. The samples were heated in a platinum pan with a heating rate of 5° C/min in order to reach final temperature. X-ray Photoelectron Spectroscopy (XPS) experiments were performed on a Physical Electronics PHI 5800 ESCA system. This system has a monochromatic Al K_α X-ray source (h_α= 1486.6 eV), hemispherical analyzer, and a multichannel detector. A low energy (30 eV) electron gun was used for the charge neutralization on the non-conducting samples. The binding energy for the samples was referenced to the C1s peak at 284.8 eV. XPSPEAK Version 4.1 peak fitting software was used to deconvolute individual peak components. Peaks were fitted using the Gaussian-Lorentizian peak profile and a Shirley background was used.

3.3. Electrochemical testing

The electrochemical performance of oxide cathodes was tested using a T-cell configuration. The active material was mixed with conducting carbon and PTFE in a 75:20:5 ratio before rolling into thin sheets. A thin sheet of lithium metal was used as the anode. 1M $LiPF_6$ [EC: EMC: DMC 1:1:1 by volume] was used as the electrolyte. The T-cells were assembled in a VAC manufactured glove box under high purity Ar gas. The T-cells were tested using an Arbin cycler under galvanostatic mode under constant current (0.1 mA/cm^2) between 4.6 V to 2 V.

4. Conclusions

We have synthesized a novel series of $(1 - x - y)LiNi_{0.8}Co_{0.2}O_2 \bullet xLi_2MnO_3 \bullet yLiCoO_2$ compounds from the ternary compositional diagram between isostructural layered $LiNi_{0.8}Co_{0.2}O_2$, Li_2MnO_3, and $LiCoO_2$ materials by well-established solid-state methods by selecting compositions that give a good representation of the composition space. Structural details were elucidated by applying Rietveld structural refinement which showed the occupation of Ni atoms in Li layers confirming the cation distribution in these types of materials. The microstructural details elucidated through SEM showed the particles are sub-micron size with interconnectivity between particles. TGA showed good thermal stability for these materials in the temperature range of study. XPS results showed that the predominant valence states of Ni, Co, and Mn are 2+, 3+, and 4+ respectively. Electrochemical testing of the samples showed the advantage of integrating the isostructural 2-D layered systems such as Li_2MnO_3 and $LiCoO_2$ resulting in increased capacity, good cyclability and considerably lower ICL. Discharge profiles showed association of redox couples Ni^{4+}/Ni^{2+} in conjunction with $Co^{4+/3+}$ (up to ~3.5 V), followed by $Mn^{4+/3+}$, up to 2V. Synthesized materials exhibit discharge capacities in the 140–230 mAh/g range, and the approach helped to identify the material with the highest capacity

RETRACTED

of 230 mAh/g corresponding to the composition of $Li_{1.2}Mn_{0.4}Ni_{0.16}Co_{0.24}O_2$. Efforts are currently underway to optimize the performance of the material further.

Acknowledgements

We thank Allan Kirkpatrick, Head, Department of Mechanical Engineering, for his continued help, support and encouragement.

References and Notes

1. Mizushima, K.; Jones, P.C.; Wiseman, P.J.; Goodenough, J.B. Li_xCoO_2 ($0 < x < 1$): A new cathode material for batteries of high energy density. *Mater. Res. Bull.* **1980**, *15*, 783–789.
2. Thomas, M.G.S.R.; David, W.I.D.; Groves, P.; Goodenough, J.B.; Groves, P. Synthesis and structural characterization of the normal spinel $Li[Ni_2]O_4$. *Mater. Res. Bull.* **1985**, *20*, 1137–1146.
3. Goodenough, J.B.; Hong, H.Y.P.; Kafalas, J.A. Fast Na^+-ion transport in skeleton structures. *Mater. Res. Bull.* **1976**, *11*, 203–220.
4. Whittingham, M.S. Electrical energy storage and intercalation chemistry. *Science* **1976**, *192*, 1126–127.
5. Tarascon, J.M.; Armand, M. Issues and challenges facing rechargeable lithium batteries. *Nature (London)* **2001**, *414*, 359–3676.
6. Thackeray, M.M.; David, W.I.F.; Bruce, P.G.; Goodenough, J.B. Electrochemical extraction of lithium from $LiMn_2O_4$. *Mater. Res. Bull.* **1989**, *19*, 179–187.
7. Padhi, A.K.; Nanjundaswamy, K.S.; Masquelier, C.; Goodenough, J.B. Mapping of transition metal redox energies in phosphates with NASICON structure by lithium intercalation. *J. Electrochem. Soc.* **1997**, *144*, 2581–2586.
8. Padhi, A.K.; Nanjundaswamy, K.S.; Goodenough, J.B. Phospho-olivines as positive-electrode materials for rechargeable lithium batteries. *J. Electrochem. Soc*. **1997**, *144*, 1188–1194.
9. Nishi, Y.; *Lithium Ion Batteries*; Wahihara, M., Yamamoto, O., Eds.; Wiley-WCH, Kodansha: Tokyo, Japan, 1988.
10. Goodneough, J.B.; Kizushima, K.; Takada, T. Solid-solution oxides for storage-battery electrodes. *Jpn. J. Appl. Phys*. **1980**, *19*, 305–313.
11. Rougier, A.; Saadoune, I.; Gravereau, P.; Willmann, P.; Delmas, C. Effect of cobalt substitution on cationic distribution in $LiNi_{1-y}Co_yO_2$ electrode materials. *Solid State Ionics* **1996**, *90*, 83–90.
12. Morales, J.; Perez-Vicente, C.; Tirado, J.L. Cation distribution and chemical deintercalation of $Li_{1-x}Ni_{1+x}O_2$. *Mater. Res. Bull.* **1990**, *25*, 623–630.
13. Dahn, J.R.; Sacken, U.; Michael, C.A. Structure and electrochemistry of $Li_{1 \pm y}NiO_2$ and a new Li_2NiO_2 phase with the Ni $(OH)_2$ structure. *Solid State Ionics* **1990**, *44*, 87–97.
14. Rougier, A.; Saadouane, I.; Gravereau, P.; Willmann, P.; Delmas, C. Effect of cobalt substitution on cationic distribution in $LiNi_{1-y}Co_yO_2$ electrode materials. *Solid State Ionics* **1996**, *90*, 83–90.
15. Saardoune, I.; Delmas, C. On the $Li_xNi_{0.8}Co_{0.2}O_2$ system. *J. Solid State Chem*. **1998**, *136*, 8–15.
16. Ohzuku, T.; Yanagawa, T.; Kouguchi, M.; Ueda, A. Innovative insertion material of $LiAl_{1/4}Ni_{3/4}O_2$ (R-3m) for lithium-ion (shuttlecock) batteries. *J. Power Sources* **1997**, *68*, 131–134.

RETRACTED

17. Armstrong, A.R.; Bruce, P.G. Synthesis of layered $LiMnO_2$ as an electrode for rechargeable lithium batteries. *Nature (London)* **1996**, *381*, 499–500.
18. Ohzuku, T.; Makimura, Y. Layered lithium insertion material of $LiNi_{0.5}Mn_{0.5}O_2$: A possible alternative to $LiCoO_2$ for advanced Lithium-ion batteries. *Chem. Lett.* **2001**, *30*, 744–745.
19. Neudecker, B.; Zuhr, R.A.; Kwak, B.S.; Bates, J.B.; Robertson, J.D. Lithium manganese nickel oxides $Li_x(Mn_yNi_{1-y})_{2-x}O_2$. *J. Electrochem. Soc*. **1998**, *145*, 4148–4159.
20. Ohzuku, T.; Makimura, Y. Layered lithium insertion material of $LiCo_{1/3}Ni_{1/3}Mn_{1/3}O_2$ for lithium-ion batteries. *Chem. Lett.* **2001**, *30*, 642–643.
21. Johnson, C.S.; Kim, J.S.; Kropf, J.; Kahaian, A.J.; Vaughey, J.T.; Fransson, L.M.L.; Edstrom, K.; Thackeray, M.M. Structural characterization of layered $Li_xNi_{0.5}Mn_{0.5}O_2$ ($0 < x < 2$) oxide electrodes for Li batteries, *Chem. Mater.* **2003**, *15*, 2313–2322.
22. Alcantara, R.; Lavela, P.; Tirado, J.L.; Zhecheva, E.; Stoyanova, R. Recent advances in the study of layered lithium transition metal oxides and their application as intercalation electrodes. *J. Solid State Electrochem*. **1999**, *3*, 121–134.
23. Stoyanova, R.; Zhecheva, E.; Zarkovam L. Effect of Mn-substitution for Co on the crystal structure and acid delithiation of $LiMn_yCo_{1-y}O_2$ solid solutions. *Solid State Ionics* **1994**, *73*, 233–234.
24. Ammundsen, B.; Paulsen, J.M. Novel Lithium-ion cathode materials based on layered manganese oxides. *Adv. Mater*. **2001**, *13*, 943–956.
25. Kim, J.S.; Johnson, C.S.; Vaughey, J.T.; Thackeray, M.M.; Hackney, S.A.; Yoon, W.; Grey, C.P. Electrochemical and structural properties of $xLi_2M'O_3 \bullet (1 - x)LiMn_{0.5}Ni_{0.5}O_2$ electrodes for lithium batteries (M' = Ti, Mn, Zr). *Chem. Mater.* **2004**, *16*, 1996–2006.
26. Shin, S.; Sun, Y.K.; Amine, K. Synthesis and electrochemical properties of $Li[Li_{(1-2x)/3}Ni_xMn_{(2-x)/3}]O_2$ as cathode materials for Lithium secondary batteries. *J. Power Sources* **2002**, *112*, 634–638.
27. Lu, Z.; Beaulieu, L.Y.; Donaberger, R.A.; Thomas, C.L.; Dahn, J.R. Synthesis, structure, and electrochemical behavior of $Li[Ni_xLi_{1/3-2x/3}Mn_{2/3-x/3}]O_2$. *J. Electrochem. Soc*. **2002**, *149*, A778–A781.
28. Wu, Y.; Manthiram, A. High capacity, surface-modified layered $Li[Li_{(1-x)/3}Mn_{(2-x)/3}Ni_{x/3}Co_{x/3}]O_2$ cathodes with low irreversible capacity loss. *Electrochem. Solid-State Lett.* **2006**, *9*, A221–A224.
29. Lu, Z.; Chen, Z.; Dahn, J.R. Lack of cation clustering in $Li[Ni_xLi_{1/3-2x/3}Mn_{2/3-x/3}]O_2$ ($0 < x \leq 1/2$) and $Li[Cr_xLi_{(1-x)/3}Mn_{(2-2x)/3}]O_2$ ($0 < x < 1$). *Chem. Mater.* **2003**, *15*, 3214–3220.
30. Yabuuchi N.; Ohzuku, T. Novel lithium insertion material of $LiCo_{1/3}Ni_{1/3}Mn_{1/3}O_2$ for advanced lithium-ion batteries. *J Power Sources* **2003**, *119*, 171–174.
31. Zhang, L.; Takada, K.; Ohta, N.; Fukuda, K.; Osada, M.; Wang, L.; Sasaki, T.; Watanabe, M. Layered $(1 - x - y)LiNi_{1/2}Mn_{1/2}O_2 \bullet xLi[Li_{1/3}Mn_{2/3}]O_2 \bullet yLiCoO_2$ cathode materials. *J. Electrochem. Soc.* **2005**, *152*, A171–A178.
32. JCPDF Standard 44-0145(for $LiCoO_2$) and 9-0063 (for $LiNi_{1-x}Co_xO_2$). International Centre for Diffraction Data: Newtown Square, PA, USA, January 2010.
33. Ohzuku, T.; Ueda, A.; Nagayama, M.; Iwakoshi Y.; Komori, H. Comparative study of $LiCoO_2$, $LiNi_{1/2}Co_{1/2}O_2$ and $LiNiO_2$ for 4 Volt secondary lithium cells. *Electrochim. Acta* **1993**, *38*, 1159.

RETRACTED

33. Rougier, A.; Gravereau, P.; Delmas, C.J. Optimization of the composition of the $Li_{1-z}Ni_{1+z}O_2$ electrode materials: Structural, magnetic, and electrochemical studies. *J. Electrochem. Soc.* **1996**, *143*, 1168–1175.
34. Shaju, K.M.; Subba Rao, G.V.; Chowdari, B.V.R. Performance of layered $Li(Ni_{1/3}Co_{1/3}Mn_{1/3}]O_2$ as cathodes for Li batteries. *Electrochim. Acta* **2002**, *48*, 145–151.
35. Liu, H.; Zhang, Z.; Gong, Z.; Yang, Y. Structural, electrochemical and thermal properties of $LiNi_{0.8-y}Ti_yCo_{0.2}O_2$ as cathode materials for lithium ion battery, *Electrochimica Acta* **2004**, *49*, 1151.
36. *CrystalMaker®: A Crystal and Molecular Structures Programs for Mac and Windows*; CrystalMaker Software Ltd.: Oxford, UK, January 2010.
37. Saadoune, I.; Delmas, C. $LiNi_{1-y}Co_yO_2$ positive electrode materials: relationships between the structure, physical properties and electrochemical behavior. *J. Mater. Chem*. **1996**, *6*, 193–199.
38. Kim, W.S.; Chung, K.; Choi, Y.K.; Sung, Y.E. Synthesis and charge-discharge properties of $LiNi_{1-x-y}$ $Co_xM_yO_2$ (M = Al, Ga) compounds. *J. Power Sources* **2003**, *115*, 101–109.
39. Wang, G.X.; Zhong, S.; Bradhurst, S.; Dou, S.X.; Liu, H.K. Synthesis and characterization of $LiNiO_2$ compounds as cathodes for rechargeable batteries. *J. Power Sources* **1998**, *76*, 141–146.
40. Endo, E.; Yasuda, T.; Yamamura, K.; Kita, A.; Sekai, K. $LiNiO_2$ electrode by chemical vapor deposition for higher voltage performance. *J. Power Sources* **2001**, *93*, 87–92.
41. Moses, A.M.; Flores, H.G.; Kim, J.G.; Langell, M.A. Surface properties of $LiCoO_2$, $LiNiO_2$ and $LiNi_{1-x}Co_xO_2$. *Appl. Surf. Sci.* **2007**, *253*, 4782–4791.
42. Galakhov, V.R.; Kurmaev, E.Z.; Uhlenbrock, S.; Newmann, M.; Kellerman, D.G.; Gorshkov, V.S. Electronic structure of $LiNiO_2$, $LiFeO_2$ and $LiCrO_2$: XPS and X-ray emission study. *Solid State Commun.* **1995**, *95*, 347–351.
43. Kalai Vani, V.; Hussain, O.M. Synthesis and characterization of electron beam evaporated $LiCoO_2$ thin films. *Ionics* **2007**, *13*, 473–477.
44. Kosova, N.V.; Devyatkina, E.T.; Kaicheve, V.V. $LiMn_2O_4$ and $LiCoO_2$ cathode materials obtained by mechanical activation. *Russ. J. Electrochem.* **2009**, *45*, 277–285.
45. Mansour, A.N. Characterization of $LiNiO_2$ by XPS. *Surf. Sci.* **1994**, *3*, 279.
46. Johnson, C.S.; Kim, J.S.; Lefief, C.; Vaughey, J.T.; Thackeray, M.M. The significance of the Li_2MnO_3 component in 'composite' $xLi_2MnO_3 \cdot (1 - x)LiMn_{0.5}Ni_{0.5}O_2$ electrodes. *Electrochem. Commun.* **2004**, *6*, 1085–1091.
47. Wiles, D.B.; Young, R.A. A new computer program for Rietveld analysis of X-ray powder diffraction patterns. *J. Applied Crystallogr.* **1981**, *14*, 149–151.
48. Roisnel, T.; Rodriguez-Carjaval J. *Fullprof Manual*; Institut Laue-Langevin: Grenoble, France, January 2010.

© 2010 by the authors; licensee MDPI, Basel, Switzerland. This article is an open-access article distributed under the terms and conditions of the Creative Commons Attribution license (http://creativecommons.org/licenses/by/3.0/).

RETRACTED